CRYSTALLIZATION

Reversible disorder-order transitions in atomic crystal nucleation

Sungho Jeon[1]*, Taeyeong Heo[1]*, Sang-Yeon Hwang[2]*†, Jim Ciston[3], Karen C. Bustillo[3], Bryan W. Reed[4], Jimin Ham[1], Sungsu Kang[5,6], Sungin Kim[5,6], Joowon Lim[1], Kitaek Lim[1], Ji Soo Kim[5,6], Min-Ho Kang[5,6], Ruth S. Bloom[4], Sukjoon Hong[1], Kwanpyo Kim[7,8], Alex Zettl[9,10,11], Woo Youn Kim[2], Peter Ercius[3]‡, Jungwon Park[5,6]‡, Won Chul Lee[1]‡

Nucleation in atomic crystallization remains poorly understood, despite advances in classical nucleation theory. The nucleation process has been described to involve a nonclassical mechanism that includes a spontaneous transition from disordered to crystalline states, but a detailed understanding of dynamics requires further investigation. In situ electron microscopy of heterogeneous nucleation of individual gold nanocrystals with millisecond temporal resolution shows that the early stage of atomic crystallization proceeds through dynamic structural fluctuations between disordered and crystalline states, rather than through a single irreversible transition. Our experimental and theoretical analyses support the idea that structural fluctuations originate from size-dependent thermodynamic stability of the two states in atomic clusters. These findings, based on dynamics in a real atomic system, reshape and improve our understanding of nucleation mechanisms in atomic crystallization.

Nucleation is a critical phenomenon in the formation of many solid materials (*1*–*3*). Classical nucleation theory describes a pathway to crystal formation (*4*, *5*) in which direct assembly of monomers occurs by density fluctuations over the surface and volume free-energy barrier. Notably, the nucleation process in diverse systems of colloidal particles (*6*, *7*), proteins (*8*, *9*), and small molecules (*10*) has been shown to incorporate nonclassical processes (*1*) such as a two-step nucleation mechanism (*2*, *3*). In those systems, metastable intermediate clusters form and then transform to stable crystals, thereby circumventing the high energy barrier of direct crystallization.

Atomic crystallization is affected by diverse metastable states, which inherently appear in small atomic clusters (~1 nm), with sizes equivalent to the nucleation stage (*11*). A few experimental studies have identified fully or partially disordered states in the early stage of atomic crystallization in solution (*12*, *13*), on surfaces (*14*, *15*), or in nanomaterials (*16*, *17*). Because of multiple local minima with similar energy levels originating from diverse metastable states (*1*, *11*), we hypothesize that the contribution of metastable states provides a dynamic nature to the early stage of crystallization. Additionally, surfaces of small clusters fluctuate because of recurrent collisions of incoming atoms and desorption of surface atoms, and thus, the free-energy barrier defining nuclei can be perturbed dynamically. These energetic interactions suggest that the early stage of atomic crystallization may exhibit nonclassical processes governed by atomistic dynamics. In this work, we investigated the heterogeneous nucleation process of gold nanocrystals on a graphene surface with atomic spatial resolution and millisecond temporal resolution.

We used three aberration-corrected transmission electron microscopes (TEMs)—one with a direct electron detector, the second with a scintillator-coupled camera combined with an electrostatic subframing system that further improved temporal resolution (*18*), and the third with a low-noise, scintillator-coupled camera for low-dose imaging (supplementary materials section 1 and fig. S1). For in situ imaging of crystal nucleation, we prepared single-layered graphene support films on which gold(I) cyanide (AuCN) nanoribbons were synthesized (fig. S2) (*19*, *20*). The electron beam acted as an imaging source as well as a reducing agent to decompose AuCN nanoribbons (~2- to 5-nm thick) to zerovalent Au atoms and $(CN)_2$ gas (*19*, *21*). The concentration of Au adatoms increased locally near the imaged nanoribbon, and the atoms aggregated to form Au nanocrystals (fig. S1A). This process occurred on the two-dimensional (2D) surface of free-standing graphene in vacuum, which minimized electron scattering from the substrate. To investigate the process from the beginning, the recording of a high-speed TEM movie was synchronized with the illumination of the high-intensity electron beam on a pristine sample area (fig. S1D). The advanced imaging detectors and sample geometry enabled us to achieve millisecond temporal resolution (1.6 and 10 ms) with atomic-scale observations.

Movie S1, with snapshots included in Fig. 1A, presents a typical high-speed TEM movie (temporal resolution: 10 ms; accelerating voltage: 300 kV; current density: 7.0×10^6 A/m^2, equivalent to an electron dose-rate of 4.4×10^5 e$^-$/Å^{2}s) of the crystal nucleation and growth processes—the overall characteristics of which are presented in the supplementary materials section 2 and fig. S3. Time-resolved investigation of each nucleation path (movie S2) elucidates that the crystal nucleation proceeds through a mechanism in which an atomic cluster transforms reversibly between disordered and crystalline states many times. As shown in the first notable events of movie S2 (Fig. 1B; seven successive frames from 140 to 200 ms), the first lattice fringe abruptly appears at 150 ms and disappears at 170 ms. Then, the second lattice fringe appears (190 ms) with a different lattice orientation and disappears at some point between 200 and 230 ms (fig. S4 and supplementary materials section 3.2). From 230 to 1190 ms, no lattice fringe is observed while strong fluctuations of pixel intensities in the center indicate the presence of an atomic cluster (Fig. 1D). Similar processes are repeated during the early stage of crystallization from 0 to ~4 s (fig. S5). Short-lived lattice fringes appear and disappear repeatedly, whereas no lattice fringe is observed in most of the frames. This phenomenon is also confirmed with multiple small peaks observed by tracking maximum intensities in 2D fast Fourier transforms (FFTs) of TEM frames over time (Fig. 1C). After ~4 s, the lattice fringe starts to grow laterally and becomes stable in the next stage of the nucleation process. Notably, this growth is not gradual, but many transitions between images that show lattice and no lattice are observed multiple times (Fig. 1, B and E). During these transitions, abrupt changes of the lattice orientation occur only when lattice fringes disappear and reappear (Fig. 1, E and F). In the final stage (after ~5 s), a stable lattice fringe gradually grows without any further abrupt changes.

The observed lattice fringes in the TEM images indicate crystalline Au nanoparticles (fig. S11). The 2D projected areas covered by lattice fringes mostly have noncircular and irregular shapes (Fig. 1B), which implies that the early-stage crystalline nuclei have nonequilibrium geometries (*16*). The frequent disappearances of existing lattice fringes, a distinguishing

[1]Department of Mechanical Engineering, BK21 FOUR ERICA-ACE Center, Hanyang University, Ansan, Gyeonggi 15588, Republic of Korea. [2]Department of Chemistry, Korea Advanced Institute of Science and Technology (KAIST), Daejeon 34141, Republic of Korea. [3]National Center for Electron Microscopy, Molecular Foundry, Lawrence Berkeley National Laboratory (LBNL), Berkeley, CA 94720, USA. [4]Integrated Dynamic Electron Solutions, Inc., Pleasanton, CA 94588, USA. [5]School of Chemical and Biological Engineering and Institute of Chemical Processes, Seoul National University, Seoul 08826, Republic of Korea. [6]Center for Nanoparticle Research, Institute for Basic Science (IBS), Seoul 08826, Republic of Korea. [7]Department of Physics, Yonsei University, Seoul 03722, Republic of Korea. [8]Center for Nanomedicine, IBS, Seoul 03722, Republic of Korea. [9]Department of Physics, University of California, Berkeley, CA 94720, USA. [10]Materials Sciences Division, LBNL, Berkeley, CA 94720, USA. [11]Kavli Energy NanoSciences Institute, Berkeley, CA 94720, USA.
*These authors contributed equally to this work. †Present address: Samsung Advanced Institute of Technology (SAIT), Samsung Electronics, Suwon 16678, Republic of Korea.
‡Corresponding author. Email: wonchullee@hanyang.ac.kr (W.C.L.); jungwonpark@snu.ac.kr (J.P.); percius@lbl.gov (P.E.)

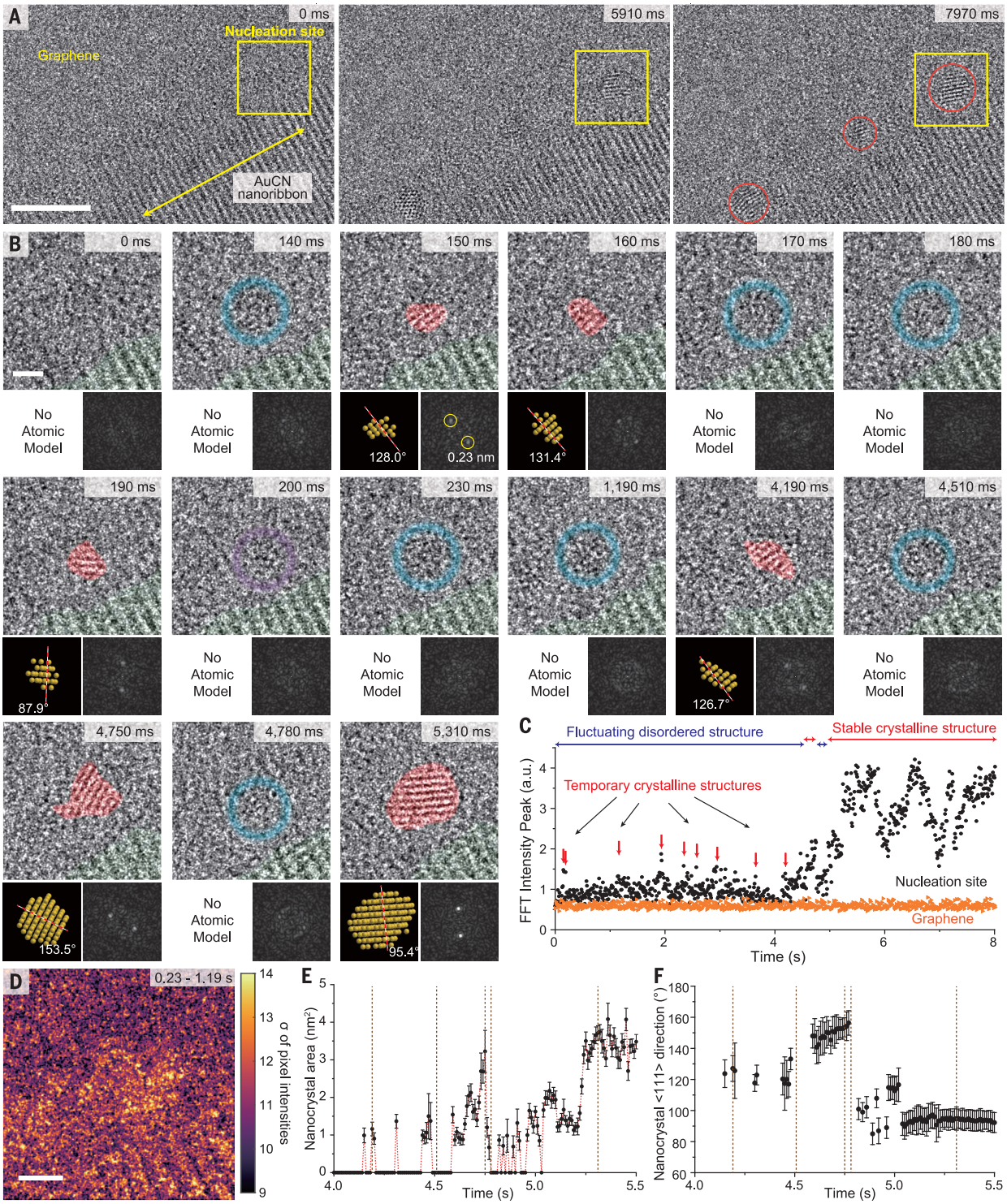

Fig. 1. Direct observation of the formation of an Au nanocrystal. (**A**) TEM image frames from the high-speed in situ movie (movie S1). Scale bar, 5 nm. Au nanocrystals in the final image are marked with red circles. (**B**) Individual frames from movie S2 showing a nucleation process [from the yellow box in (A); temporal resolution, 10 ms]. Beneath each frame on the left side, an atomic model of the nanocrystal is shown. Red dashed lines indicate nanocrystal <111> directions. Beneath each frame on the right, an FFT image is shown. Scale bar, 1 nm. The areas of Au lattices and AuCN nanowires in the frames are pseudocolored in red and light-green, respectively. Blue circles indicate nanoclusters in the disordered state, and purple circles indicate the undefinable state (where the crystalline versus disordered classification is unclear). (**C**) Maximum intensity of the FFT image as a function of time. The signals from a graphene area represent ground noise levels (negative control) of this analysis. a.u., arbitrary units. (**D**) A color map obtained from standard deviations of intensities from 230 to 1190 ms for each pixel. Scale bar, 1 nm. (**E**) Nanocrystal area from 4.00 to 5.50 s. (**F**) Direction of <111> lattices from 4.00 to 5.50 s. Vertical dotted lines in (E) and (F) correspond to the time-labeled images in (B). Related images and detailed methods are presented in figs. S3 to S10.

observation in this study, can be interpreted as a transformation of crystalline atomic structures to a disordered state. This analysis is derived from previous works which have identified fluctuating disordered (*22*, *23*) or quasi-melting (*24*) states of nanoclusters. TEM frames without a lattice fringe instead show continuous fluctuations of granular features with sizes commensurate with those of Au atoms (Fig. 1D, fig. S10, and movie S2, 0.23 to 1.19 s), and similar series of TEM frames were presented as evidence of previous identifications of disordered states (*22*–*24*). Previous x-ray diffraction (XRD) analyses confirmed disordered atomic structures of small Au nanoparticles (less than ~2 nm) (*25*). The presence of disordered atomic clusters in our case is also supported by Fig. 1, E and F, which shows that lattice orientations abruptly changed only after they disappeared and reemerged. We can rule out other explanations for the lattice disappearance (supplementary materials section 3.1), such as the tilting of nanocrystals away from low-index zone axes or the fast rotation of nanocrystals within our exposure time (~10 ms). Small nanocrystals (less than ~2 nm) always present lattice fringes in high-resolution TEM images regardless of viewing orientations (*22*, *26*), confirmed by TEM image simulations (fig. S12). The fast rotation of a nanocrystal inherently changes lattice orientations (fig. S13), but our TEM movies show that lattice orientations are fixed in successive frames during which crystalline domains decrease in size and then disappear (fig. S14).

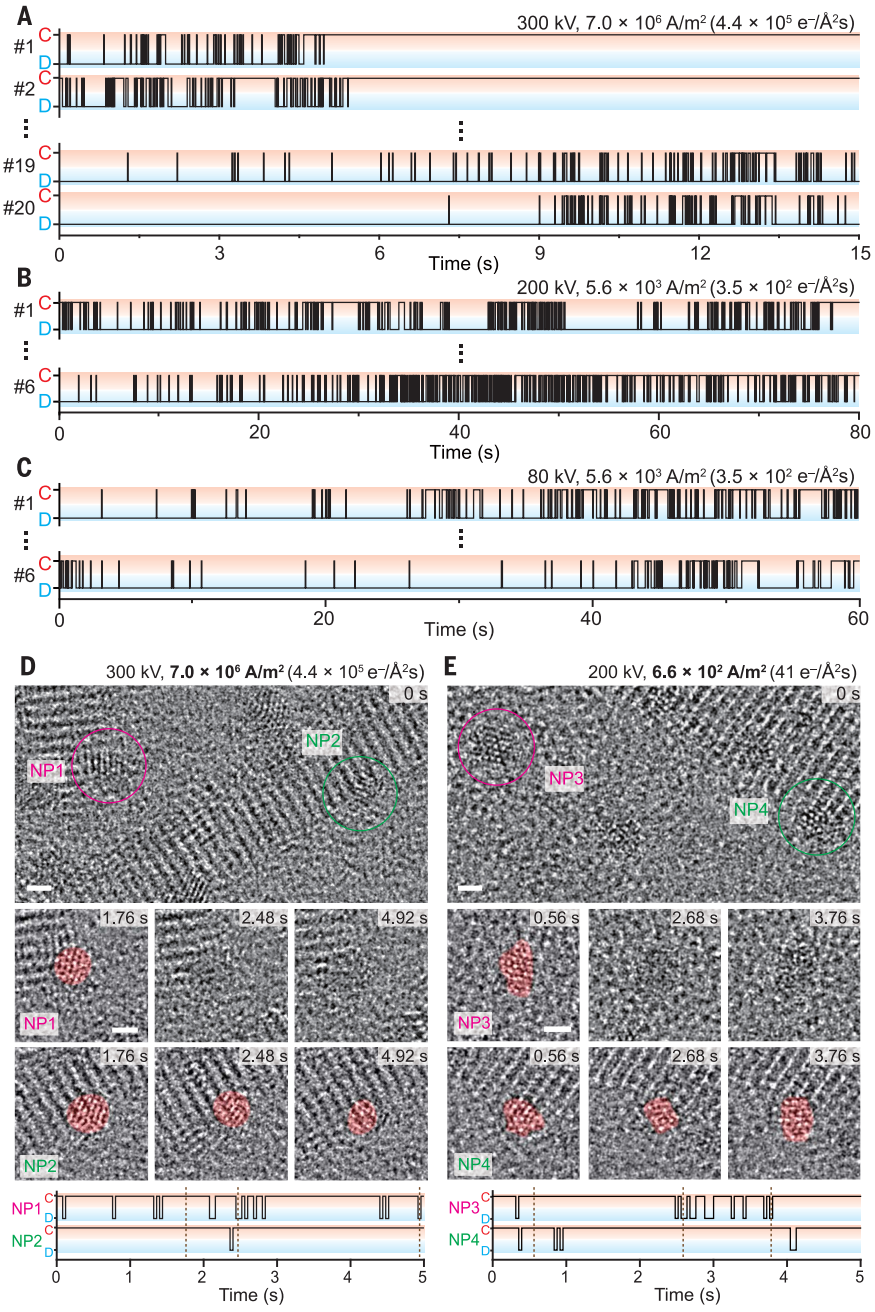

Fig. 2. Multiple nucleation paths of Au nanocrystals. (**A** to **C**) Trajectories of structural transitions between disordered and crystalline states in multiple nucleation paths observed at 300 kV and 7.0 × 10^6 A/m^2 (A), at 200 kV and 5.6 × 10^3 A/m^2 (B), and at 80 kV and 5.6 × 10^3 A/m^2 (C). Red and blue shadings are visual guides for indicating crystalline (labeled C) and disordered (labeled D) states, respectively. The first nucleation path (#1) in (A) is the dataset in Fig. 1. (**D** and **E**) TEM images and trajectories of structural transitions showing asynchronized structural fluctuations of two neighboring nanoclusters observed at 300 kV and 7.0 × 10^6 A/m^2 (D) and at 200 kV and 6.6 × 10^2 A/m^2 (E). The two cases have four orders of magnitude difference in current density. Scale bars, 1 nm. NP, nanoparticle.

On the basis of the above analysis, the process shown in Fig. 1 can be described as a trajectory of recurrent structural transformations between disordered and crystalline states, which is nucleation path 1 in Fig. 2A. In the early stage, a gold nanocluster is mostly in the disordered state and fluctuates continuously, while a few short-lived crystalline states appear with a relatively short lifetime. Repeated transformations between the two states are observed for an extended period, and ultimately a stable crystalline particle is formed. Slowing down the effective frame rate of movie S1 with frame-averaging to the previously achievable level of conventional TEM (fig. S3; 0.5 s per frame) greatly improves the signal-to-noise ratio of each TEM image, but the frame-averaged movie incorrectly suggests that the process follows a sequence of irreversible steps: A blurry or granular spot forms at the nucleation site (0.5 to 1.0 s), then the spot transforms into a lattice fringe (4.5 to 5.0 s), and the lattice fringe gradually grows. However, our high-speed in situ observations reveal that the process includes dynamic and reversible transformations between the two states.

The characteristics discovered in Fig. 1 are consistently observed in all nucleation paths investigated in this study (figs. S15 to S29 and movies S3 to S5). We modified the electron beam conditions (fig. S15) to control kinetic factors and affect the nucleation process. For example, the rate of Au adatom supply determined by radiolysis of AuCN was found to be sensitive to accelerating voltage and current density. Radiolysis of AuCN was highest at 80 kV and decreased with lower current densities (fig. S30 and supplementary materials section 4.2). We performed in situ imaging

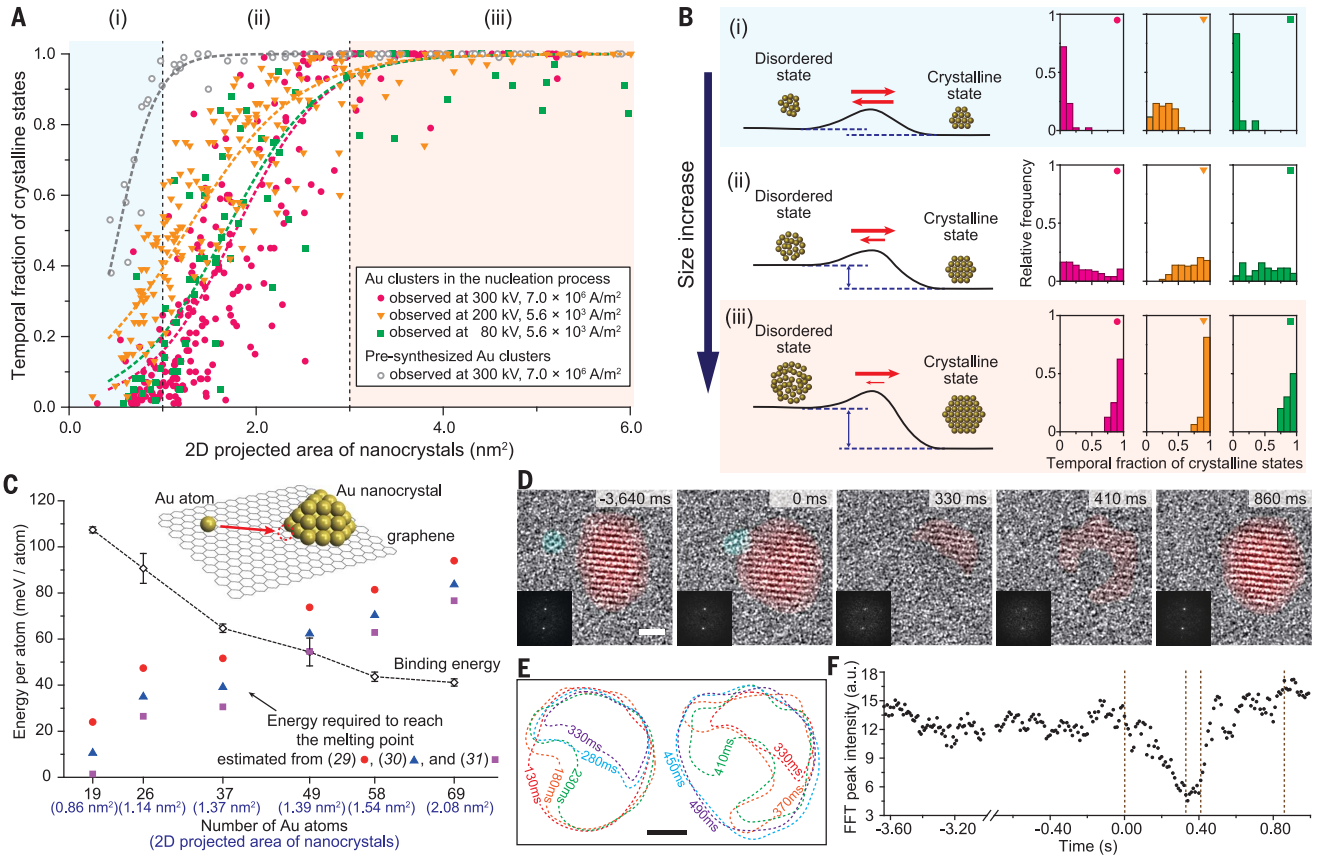

Fig. 3. Experimental and theoretical investigations of the crystalline-to-disordered transformations during the nucleation process. (**A**) Temporal fraction of crystalline states versus 2D projected area of Au nanocrystals observed during the nucleation processes (solid symbols) and observed using presynthesized Au nanoclusters (gray circles). The dashed curves represent fitting lines to the data with sigmoid (logistic) functions. (**B**) Size-dependent characteristics of nanoclusters during the nucleation process. (Left) Schematic energy diagrams showing the nucleation mechanisms of nanocrystals from small (i) to large (iii) sizes. (Right) Histograms of the temporal fractions of crystalline states for three size ranges (0 to 1.0 nm^2, 1.0 to 3.0 nm^2, and 3.0 to 6.0 nm^2) and three different imaging conditions indicated in (A). (**C**) First-principles calculations of the binding energy between an Au atom and hemispheroidal Au$_n$ nanocrystals. The binding energy is compared with the energy required to reach the melting point of Au$_{n+1}$ nanocrystals. (Inset) Binding model at n = 37. (**D**) Sequential TEM images showing the binding of a small nanocluster (colored in blue) to a large nanocrystal (colored in red). (Insets) FFT images of the nanocrystal. (**E**) Time-labeled contour plots of crystalline areas during partial collapse (left) and recrystallization (right). (**F**) Maximum intensities of the FFT images. Vertical dotted lines and axis in (F) correspond to the time-labeled images in (D), respectively. Scale bars, 1 nm.

under seven different conditions (fig. S15) with accelerating voltages of either 80, 200, or 300 kV and current densities ranging from 6.6×10^2 A/m^2 (41 e$^-$/Å^{2}s) to 6.1×10^7 A/m^2 (3.8×10^6 e$^-$/Å^{2}s). The best temporal resolution achieved was 1.6 ms (at 200 kV and 6.1×10^7 A/m^2) using a subframing system (fig. S1C and fig. S25). Thus, we investigated nucleation paths in a wide range of the averaged growth rate of Au nanoclusters, from ~0.5 atoms per second (at 200 kV and 6.6×10^2 A/m^2) to ~50 atoms per second (at 80 kV and 5.9×10^5 A/m^2; at 200 kV and 6.1×10^7 A/m^2). Regardless of the different conditions, the existence of dynamic structural fluctuations during the nucleation process is confirmed in all 68 nucleation paths, as shown in the nucleation paths under three representative conditions in Fig. 2, A to C. Additionally, structural fluctuations of neighboring nanoclusters occur asynchronously in each of the in situ movies, and these phenomena are consistently observed under substantially different conditions (Fig. 2, D and E). It further supports that stochastic structural fluctuations are universal in the observed nucleation process (supplementary materials section 4.4).

Using the multiple nucleation paths presented in Fig. 2, A to C, we performed a statistical analysis for the relative population between the disordered and crystalline states, which is indicative of the relative stability of the two states. For example, from the 20 nucleation paths in Fig. 2A and fig. S22, we calculated temporal fractions of the crystalline state (fig. S31) and investigated their relation to the sizes of nanocrystals (magenta dots in Fig. 3A). The other two cases (Fig. 2, B and C), which had current densities 10^{-3} times that of the first case, were also analyzed with the identical method (orange triangles and green squares in Fig. 3A). The results from different conditions follow a similar trend, and the difference is relatively small, as seen in the scattering of the data points. In all three cases, a nascent small nanocluster has a high probability of retaining the disordered state (top part in Fig. 3B). Then, the relative population of the crystalline state increases while the nanocluster grows from ~1.0 to ~3.0 nm^2 (middle part in Fig. 3B; equivalent circular diameters: ~1.1 to ~2.0 nm). Eventually, the enlarged nanocluster maintains the crystalline state (bottom part in Fig. 3B). This implies that the observed process is an evolution of atomic structures through stochastic and dynamic fluctuations between two states with size-dependent relative stability. Figure 3A also indicates that the observed structural fluctuations are mainly directed by the formation and

early-stage growth of nanoclusters and are not an artifact induced by the electron beam. The electron beam can transfer a certain amount of energy to Au atoms and clusters elastically and/or inelastically, which may generate the crystalline-to-disordered transformations of clusters. To confirm that this was not the case in our study, Au nanoclusters smaller than 2 nm were prepared by a typical colloidal synthesis and observed under the same imaging condition for a prolonged time (supplementary materials section 4.1). Small-sized presynthesized clusters occasionally show disordered structures (fig. S32), consistent with previous studies (*22*–*28*). However, Fig. 3A indicates that the presynthesized clusters (gray circles) were mostly in the crystalline state throughout imaging for cluster sizes larger than ~1 nm, which is clearly different from the other cases (solid symbols) observed during the nucleation process. Additionally, extensive discussion regarding the electron beam effects is provided in the supplementary materials section 4 (figs. S15, S16, and S25 to S34).

The free-energy change for the transition from disordered to crystalline states is usually negative and large enough to make the transition spontaneous. However, statistical observations of the reversible and dynamic transformations in Fig. 3, A and B, imply that the energy difference and the barrier between the two states are small when the cluster size is small in the early stage of nucleation (top part in Fig. 3B). As nanoclusters grow, the energy difference gradually increases, and the nanoclusters present the crystalline state more frequently. From a certain nanocluster size (~2.0 nm in our study), nanoclusters are trapped in the crystalline state because of the increased energy difference (bottom part in Fig. 3B). Many theoretical and experimental studies (*22*–*28*) have reported that small (less than ~2 nm) nanoparticles can have disordered atomic structures even in ambient conditions. Melting-point depression (*29*–*31*) also means that crystalline-to-disordered transitions require substantially reduced energy in small nanoparticles compared with bulk materials. These previous results consistently support the low energy barrier of the crystalline-to-disordered transformation of small nanoclusters. Fluctuations between two states over a free-energy barrier are a key thermodynamic concept of classical nucleation theory. Although this concept is not excluded in the framework of nonclassical two-step nucleation (fig. S35) (*2*), only a few studies (*7*, *17*, *32*) have investigated it. The above thermodynamic description and our high-speed observations reintroduce and verify the idea that reversible and dynamic transformations can occur in nonclassical nucleation pathways.

The low energy barrier of the crystalline-to-disordered transformation can be overcome by various sources. Monomer attachment is an exergonic reaction and can deposit a relatively large amount of energy to nascent nanoclusters as thermal fluctuations and the electron beam can. We performed first-principles calculations of the energy released from binding reactions between an Au atom and hemispheroidal Au nanocrystals (Fig. 3C, figs. S36 and S37, tables S1 to S3, and supplementary materials section 5), and we evaluated whether the calculated energies are comparable to collapsing crystalline structures by using the thermal energies required to increase the temperatures of the nanocrystals to the depressed melting points (*29*–*31*). The crossover of the two energies occurs at the nanocrystal size containing 49 constituent atoms (nanocrystal area: ~1.4 nm^2) in Fig. 3C. This implies that recurrent binding of Au atoms can provide sufficient energy to small clusters to drive toward the disordered state. Experimental results that partly support this hypothesis are presented in Fig. 3, D to F; fig. S38; and movie S6, which show that the binding of a small atomic cluster (composed of ~10 atoms, ~0.7 nm^2) to a large nanocrystal induces noticeable structural transformations to the disordered state. Just after the atomic-cluster binding, the crystalline area is gradually reduced and then recovered (~9.0 nm^2 → ~3.0 nm^2 → ~10.0 nm^2). We also found that coalescence of small nanocrystals drives either or both of the nanocrystals to visit the disordered state (figs. S39 to S43 and movie S7). Therefore, reversible transformations commonly occur throughout various stages in our model system. Our system does not universally reproduce the entire scope of crystal nucleation starting from scattered monomers. However, our work reveals near-atomic scale dynamics from concentrated adatoms to the formation of a stable crystal, thereby addressing a critical step that determines the nucleation pathway in many different types of crystallization processes (supplementary materials section 6 and fig. S44).

In this study, we found that crystal nucleation of gold clusters on graphene progresses through reversible structural fluctuations between disordered and crystalline states. High-speed in situ observations of a real atomic system confirm nonclassical and dynamic natures of the nucleation process during atomic crystallization. Our findings clarify fundamental mechanisms underlying the nucleation stage of material growth, including thin-film deposition, interface-induced precipitation, and nanoparticle formation.

REFERENCES AND NOTES

1. J. J. De Yoreo *et al.*, *Science* **349**, aaa6760 (2015).
2. P. G. Vekilov, *Cryst. Growth Des.* **10**, 5007–5019 (2010).
3. D. Erdemir, A. Y. Lee, A. S. Myerson, *Acc. Chem. Res.* **42**, 621–629 (2009).
4. J. Chen *et al.*, *Science* **362**, 1135–1139 (2018).
5. M. Sleutel, J. Lutsko, A. E. S. Van Driessche, M. A. Durán-Olivencia, D. Maes, *Nat. Commun.* **5**, 5598 (2014).
6. Z. Ou, Z. Wang, B. Luo, E. Luijten, Q. Chen, *Nat. Mater.* **19**, 450–455 (2020).
7. T. H. Zhang, X. Y. Liu, *Angew. Chem. Int. Ed.* **48**, 1308–1312 (2009).
8. P. R. ten Wolde, D. Frenkel, *Science* **277**, 1975–1978 (1997).
9. L. Houben, H. Weissman, S. G. Wolf, B. Rybtchinski, *Nature* **579**, 540–543 (2020).
10. M. H. Nielsen, S. Aloni, J. J. De Yoreo, *Science* **345**, 1158–1162 (2014).
11. A. S. Barnard, N. P. Young, A. I. Kirkland, M. A. van Huis, H. Xu, *ACS Nano* **3**, 1431–1436 (2009).
12. N. D. Loh *et al.*, *Nat. Chem.* **9**, 77–82 (2017).
13. J. Yang *et al.*, *J. Am. Chem. Soc.* **141**, 763–768 (2019).
14. M. H. Hu, S. Noda, H. Komiyama, *J. Appl. Phys.* **93**, 9336–9344 (2003).
15. L. Fei *et al.*, *ACS Nano* **13**, 681–688 (2019).
16. J. Zhou *et al.*, *Nature* **570**, 500–503 (2019).
17. K. Cao *et al.*, *Nat. Chem.* **12**, 921–928 (2020).
18. B. W. Reed *et al.*, *Struct. Dyn.* **6**, 054303 (2019).
19. W. C. Lee *et al.*, *Nat. Nanotechnol.* **10**, 423–428 (2015).
20. J. Kim *et al.*, *J. Phys. Chem. Lett.* **8**, 1302–1309 (2017).
21. M. T. Beck *et al.*, *J. Solid State Chem.* **246**, 65–74 (2017).
22. Z. W. Wang, R. E. Palmer, *Nano Lett.* **12**, 5510–5514 (2012).
23. T. J. Pennycook, J. R. McBride, S. J. Rosenthal, S. J. Pennycook, S. T. Pantelides, *Nano Lett.* **12**, 3038–3042 (2012).
24. P. M. Ajayan, L. D. Marks, *Phys. Rev. Lett.* **63**, 279–282 (1989).
25. V. Petkov *et al.*, *J. Phys. Chem. C* **112**, 8907–8911 (2008).
26. L. Li *et al.*, *J. Am. Chem. Soc.* **135**, 13062–13072 (2013).
27. Y. Sun, L. Zhuang, J. Lu, X. Hong, P. Liu, *J. Am. Chem. Soc.* **129**, 15465–15467 (2007).
28. I. L. Garzón *et al.*, *Phys. Rev. Lett.* **81**, 1600–1603 (1998).
29. P. Buffat, J. P. Borel, *Phys. Rev. A* **13**, 2287–2298 (1976).
30. K. Dick, T. Dhanasekaran, Z. Zhang, D. Meisel, *J. Am. Chem. Soc.* **124**, 2312–2317 (2002).
31. W. H. Qi, M. P. Wang, *Mater. Chem. Phys.* **88**, 280–284 (2004).
32. P. W. Sutter, E. A. Sutter, *Nat. Mater.* **6**, 363–366 (2007).

ACKNOWLEDGMENTS

The authors thank A. Minor, T. Hyeon, S. Takeuchi, and S. Chung for helpful discussions. **Funding:** This work was mainly supported by the National Research Foundation of Korea (NRF) funded by the Ministry of Science and ICT (MSIT) and the Ministry of Education (MOE) under contract nos. 2016R1C1B1014940 and 2019R1F1A1059099. Work at the Molecular Foundry was supported by the Office of Science, Office of Basic Energy Sciences, of the U.S. Department of Energy under contract no. DE-AC02-05CH11231. The authors also acknowledge multiple financial supports from the Institutes for Basic Science (IBS-R006-D1); the NRF funded by the Korean government (MSIT and MOE) under contract nos. 2017R1C1B2010434, 2017R1A5 A1015365, 2019M3E6A1064877, 2018R1A5A1025208, 2017R1A5A1014862, 2015M3C1B2052811, 2018R1D1A1B07050575, and 2020R1F1A1065856; the Samsung Science and Technology Foundation for developing the data analysis and TEM simulation methods (M.-H.K. and J.P., no. SSTF-BA1802-08); the U.S. Department of Energy, Office of Science, Office of Basic Energy Sciences, Materials Sciences and Engineering Division (DE-AC02-05-CH11231) within the Nanomachines Programs (KC1203), which supported preliminary TEM measurements; and the U.S. National Science Foundation (DMR-1807233), which provided for the development of graphene TEM supports. **Author contributions:** W.C.L., J.P., and P.E. conceived the design of the study. S.J., S.Ka., J.C., K.C.B., B.W.R., R.S.B., P.E., and W.C.L. performed in situ TEM imaging. S.J. and T.H. analyzed the data. S.-Y.H. and W.Y.K. performed first-principles calculations. J.S.K., J.H., S.Ki., J.L., K.L., M.-H.K., S.H., K.K., and A.Z. contributed to sample preparation or data analysis. S.J., T.H., S.-Y.H., J.C., K.C.B., B.W.R., S.H., P.E., J.P., and W.C.L. wrote the manuscript. All authors discussed the results and commented on the manuscript. **Competing interests:** The authors declare no competing interests. **Data and materials availability:** All data are available in the main text or the supplementary materials.

SUPPLEMENTARY MATERIALS

science.sciencemag.org/content/371/6528/498/suppl/DC1
Materials and Methods
Supplementary Text
Figs. S1 to S44
Tables S1 to S3
References (*33*–*65*)
Movies S1 to S7

15 October 2019; resubmitted 19 October 2020
Accepted 28 December 2020
10.1126/science.aaz7555

Science

Reversible disorder-order transitions in atomic crystal nucleation

Sungho Jeon, Taeyeong Heo, Sang-Yeon Hwang, Jim Ciston, Karen C. Bustillo, Bryan W. Reed, Jimin Ham, Sungsu Kang, Sungin Kim, Joowon Lim, Kitaek Lim, Ji Soo Kim, Min-Ho Kang, Ruth S. Bloom, Sukjoon Hong, Kwanpyo Kim, Alex Zettl, Woo Youn Kim, Peter Ercius, Jungwon Park and Won Chul Lee

Science **371** (6528), 498-503.
DOI: 10.1126/science.aaz7555

Watching early stage nucleation

In classic nucleation theory, a metastable disordered dense liquid or amorphous solid cluster spontaneously and irreversibly transforms into a crystalline nucleus. Jeon *et al.* observed the formation of gold crystals on a graphene substrate through the reduction of a precursor using an electron beam. Rather than the classic view, they instead observed a nucleation pathway that involves dynamic and reversible fluctuations of developing nuclei between disordered and crystalline states. The lifetime in the disordered state decreases with increasing cluster size, and at sufficiently small sizes, the binding energy per atom is large enough relative to the energy required to induce melting that the heat imparted upon binding is enough to drive partial collapse of an ordered cluster into the disordered state.

Science, this issue p. 498